

NASA TR R-142

NATIONAL AERONAUTICS AND SPACE ADMINISTRATION

TECHNICAL REPORT
R-142

EFFECT OF LARGE-AMPLITUDE OSCILLATIONS ON HEAT TRANSFER

By CHARLES E. FEILER and ERNEST B. YEAGER

1962

For sale by the Superintendent of Documents, U.S. Government Printing Office, Washington 25, D.C. Yearly subscription, $15; foreign, $19; single copy price varies according to size ---------- Price 40 cents

TECHNICAL REPORT R-142

EFFECT OF LARGE-AMPLITUDE OSCILLATIONS ON HEAT TRANSFER

By CHARLES E. FEILER and ERNEST B. YEAGER

Lewis Research Center
Cleveland, Ohio

TECHNICAL REPORT R-142

EFFECT OF LARGE-AMPLITUDE OSCILLATIONS ON HEAT TRANSFER[1]

By CHARLES E. FEILER and ERNEST B. YEAGER

SUMMARY

The heat transfer from a heated flat plate to an airstream having large-amplitude flow oscillations or a high degree of free-stream turbulence was studied. The frequency of the oscillation was varied from 34 to 680 cps at root-mean-square flow amplitudes of as much as 65 percent of the mean flow rate. For both oscillatory and turbulent flows, the heat-transfer coefficient was larger than that predicted by established relations in the literature. The Nusselt number with oscillations was as much as 65 percent larger than that with the reference flow at the same Reynolds number. The Nusselt number was correlated by a function of the Reynolds number and the ratio of the root-mean-square amplitude of the velocity excursions to the mean flow rate for both kinds of flow.

No effect of oscillation frequency was observed that could be attributed solely to frequency over the range that frequency was varied. Schlieren studies of the thermal boundary layer revealed that flow reversal occurred near the plate surface at each frequency and also that the temperature profile followed a periodic behavior. The time-averaged value of the thermal-boundary-layer thickness (given by the distance at which the temperature gradient attained a prescribed value) varied inversely with the Nusselt number.

Although, in the oscillatory flow, the oscillations had a definite periodicity while, in the turbulent flow, the oscillations were strictly random, the mechanism by which heat transfer was increased appeared to be the same in both flows. The mechanism appeared to be associated with turbulence and the transfer of energy from the free stream into the boundary layer.

[1] The information presented in this report was offered by Dr. Charles E. Feiler as a thesis in partial fulfillment of the requirements for the degree of Doctor of Philosophy in Physical Chemistry, Western Reserve University, Cleveland, Ohio, September 1961. Professor Ernest B. Yeager was faculty advisor.

INTRODUCTION

In recent years there has been a growing interest in the effects of flow oscillations and sound waves on momentum and energy transport phenomena. It has been observed generally that oscillations of sufficient intensity are capable of altering the rates of these transport processes, presumably by virtue of the nonlinear nature of the interaction. Both forced- and natural-convection effects have been studied in the literature. With natural convection, steady flows called acoustic streaming flows may be produced in the vicinity of the body, which may result in an increase in the heat-transfer rate. An analysis of this case has been made that predicts the critical sound-pressure level necessary to increase the heat-transfer rate (ref. 1). Large bibliographies pertaining to acoustic streaming and heat transfer may be found in references 2 and 3.

As the net flow velocity is increased, streaming flows become negligible with respect to the overall velocity, and the mechanism by which the heat-transfer rate is increased is different. An analysis of the effects of free-stream oscillations on boundary-layer flow indicates that the boundary layer behaves qualitatively the same as it does in the presence of free-stream turbulence (ref. 4). Other theoretical analyses of the effects of oscillations on boundary layers have demonstrated that the skin friction and heat-transfer rate undergo phase shifts with respect to the free-stream oscillation (refs. 5 and 6). In general, these analyses predict little change or even a decrease in the heat-transfer rate presumably due to the small amplitude to which they are necessarily restricted.

Experimentally, it has been found that oscillations superimposed on the mean flow produce an increase in the heat-transfer rate for several different test systems in both air and water (refs. 7 to 13). In general, the increase in the heat-

transfer rate has been found to depend on the velocity amplitude rather than the pressure amplitude. In some cases the increase also depended on the frequency. The correlations that have been obtained are largely empirical. In view of the wide variety of flow conditions that are possible, it appears that considerable work will be required to consolidate the physical laws governing these phenomena.

It was the purpose of this investigation to examine the heat-transfer process from a simple body to an airstream having a large-amplitude oscillation superimposed on it. Accordingly, a flat plate was selected, and its rate of heat transfer was measured in an oscillating flow. Qualitative studies of the boundary layer on the plate were made by the schlieren technique. From the experimental results, a correlation of the heat-transfer coefficients with flow parameters was obtained, which indicates the parameters of importance and the dependence of heat-transfer coefficient upon them.

SYMBOLS

A area ribbon surface, sq ft

B proportionality constant (eq. (12)), dimensionless

C_p heat capacity, Btu/(lb)(°F)

D horizontal displacement of wire image (fig. 6), in.

$\overline{e^2}$ mean square of total fluctuating hot-wire voltage due to turbulence

$\overline{\Delta e^2}$ mean square of fluctuating hot-wire voltage between frequencies, $f+\Delta f/2$ and $f-\Delta f/2$

$F(f)$ fraction of turbulent energy associated with frequency, $F(f)=\dfrac{\overline{\Delta e^2}}{\overline{e^2}\,\Delta f}$

f focal length of schlieren mirrors, in.

f_1, f_2' functions of ϵ (eq. (13))

f_2 function of ϵ (eq. (17))

f frequency, cps

Δf effective bandwidth of harmonic wave analyzer, 4.5 cps

g function

h local heat-transfer coefficient, Btu/(hr)(sq ft)(°F)

k thermal conductivity, Btu/(hr)(sq ft)(°F/ft)

L optical path length (fig. 6), in.

M exponent (eq. (12))

m magnification factor of schlieren objective lens system (fig. 6)

n constant (eq. (26))

dn/dy refractive index gradient normal to plate surface, radians/in.

P pressure, lb/sq in. gage

q heat-transfer rate, Btu/hr

q_{cond} heat-transfer rate by conduction, Btu/hr

q_{conv} heat-transfer rate by convection, Btu/hr

q_{gen} rate of heat generation, Btu/hr

q_{rad} heat-transfer rate by radiation, Btu/hr

T temperature, °F

ΔT temperature difference between plate surface and airstream, °F

$\Delta T'$ temperature difference between plate surface and airstream defined by eq. (25), °F

t time, sec

V air velocity in x-direction, ft/sec

x distance along plate in flow direction measured from leading edge, in.

Δx horizontal displacement (fig. 6), in.

x_L distance from leading edge of plate to first heater ribbon, in.

y distance normal from plate surface, in.

Δy vertical displacement (fig. 6), in.

α angle of inclination of inclined wire (fig. 6), deg

δ thickness of thermal boundary layer, in.

θ angle of refraction of light rays (fig. 6), radians

λ period of oscillation, sec

μ viscosity coefficient, lb/(ft)(sec)

ρ density, lb/cu ft

ρV weight-flow rate per unit area, (lb)/(sq ft)(sec)

σ standard deviation

τ_o wall shear stress, lb/(ft)(sec)^2

Dimensionless groups:

Nu_x Nusselt number, hx/k

Pr Prandtl number, $C_p\mu/k$

Re_x Reynolds number, $\rho Vx/\mu$

$\overline{V}^+$ velocity parameter, $\overline{V}/\sqrt{\tau_o/\rho}$

y^+ wall distance parameter, $\dfrac{\sqrt{\tau_o/\rho}}{\mu/\rho}\,y$

ϵ amplitude parameter or turbulence intensity, $(\rho V)_{rms}/\overline{\rho V}$

Subscripts:

cal calibration

f with oscillations

i instantaneous

o without oscillations
rms root-mean-square
Superscript:
$(-)$ time-averaged value

APPARATUS

The object of this work was to investigate experimentally the effect of flow oscillations on forced-convection heat transfer. Because of the relatively large steady-state flow velocity planned, it was anticipated that very high sound levels would be necessary to influence the heat-transfer rates appreciably. A review of the literature for methods of producing such levels indicated that the siren offered the best means of achieving this goal. The siren also affords an easy way to vary the frequency of sound over a wide range.

For the test specimen a flat plate was selected. The flat plate appeared to have a simpler flow field than a cylinder and was more adaptable to visual boundary-layer studies than the boundary layer in pipe flow.

Finally, since it was expected that velocity amplitude, rather than pressure amplitude, would be the most important parameter affecting heat transfer, the hot-wire anemometer was selected for measuring the flows. The hot-wire anemometer has an upper frequency response of the order of 50,000 cps and is thus capable of measuring instantaneous flows over a considerable range.

SIREN

The siren used to produce the oscillations is shown in figures 1 and 2. The siren stator has 20 ports, and the rotor has 20 matching blades. The rate of change of port area is linear, and there is no dwell time in the fully open or fully closed positions. The downstream or outlet side of the stator was designed with a splitter plate between each port and a spinner in the center hub section. These were intended to minimize the losses in sound power due to turbulence generation caused by the sudden expansion of the flow on passing through the ports.

It was considered desirable to have the effective area of the siren as large as possible to ensure that the sound waves would be plane-fronted. Also, the larger this area is, the smaller is the reduction in sound power due to expansion into the duct. The area of each port was about 1 square inch so that the total area was 20 square inches or 0.4 of the duct cross-sectional area. The outside diameter of the ports was equal to the inside diameter of the duct.

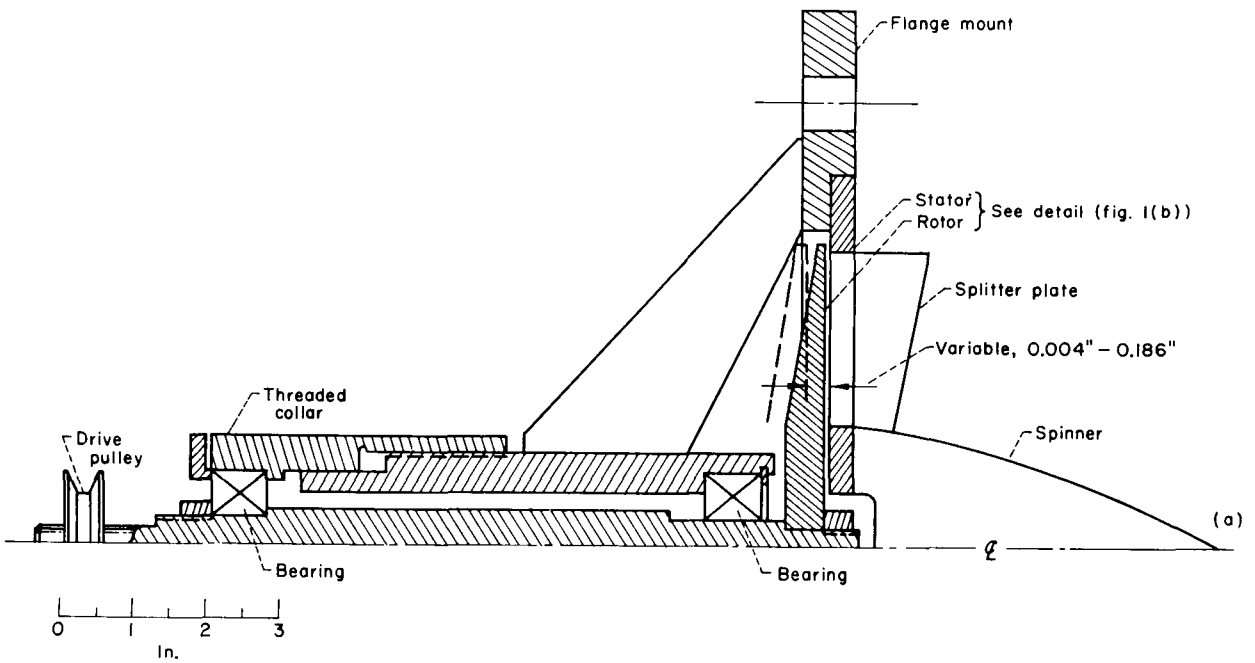

(a) Cross section.

FIGURE 1.—Siren detail.

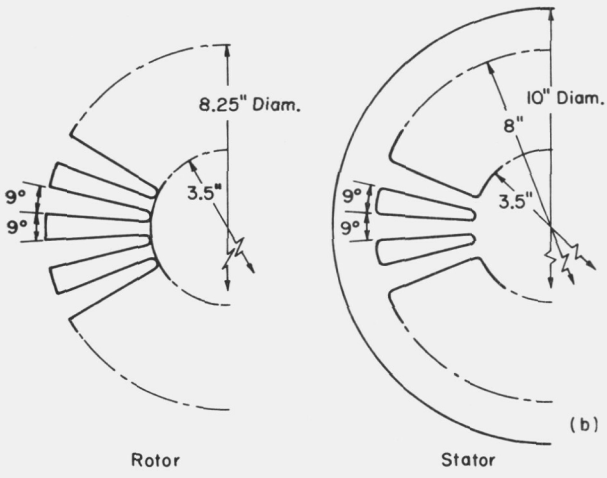

(b) Rotor and stator detail.

FIGURE 1.—Concluded. Siren detail.

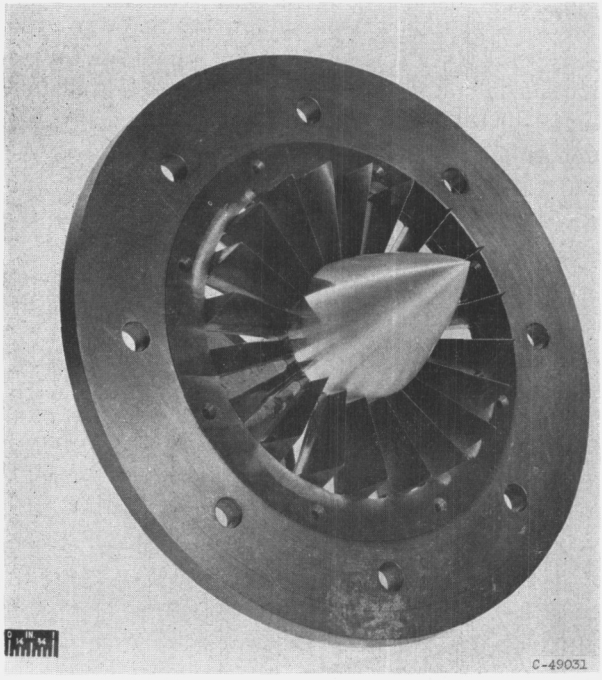

FIGURE 2.—Siren assembly.

Clearance between the rotor and stator was adjustable by means of a vernier thread from 0.004 to 0.186 inch. The outside diameter of the rotor was 0.25 inch larger than the outside diameter of the stator ports. In this way an air-film bearing was provided at the circumference of the rotor, making contact with the stator difficult. The rotor was belt-driven by a ½-horsepower direct-current compound motor rated at 1700 rpm. By controlling the voltage applied to the shunt field and armature windings of the motor, it was possible to vary the speed from 100 to 2400 rpm corresponding to oscillation frequencies from 34 to 800 cps.

FLAT PLATE AND HEATING CIRCUIT

A sketch of the plate is shown in figure 3. The body was constructed of Bakelite with a sharp leading edge and was 0.5 inch thick, 6 inches long, and 4 inches wide. Nichrome ribbons 0.002 inch thick, 0.5 inch wide, and 3 inches long were mounted transversely and flush on the upper surface of the plate. The five ribbons were spaced 0.06 inch apart starting 1 inch from the leading edge. The plate extended 0.5 inch beyond the ends of the ribbons. All the power leads and thermocouple leads were contained in the body of the plate and its mount. Five No. 36 B. & S. gage iron-constantan thermocouples were spotwelded to the lower surface of each ribbon at the center and at distances of ⅜ and 1 inch on either side of the center. Two thermocouples were also placed on the lower surface of the Bakelite at a known distance from the upper surface. The thermocouples were all referenced to a free-stream thermocouple by means of a multiposition switch. In this way only temperature differences were measured. The thermocouples were calibrated against a standard, and their sensitivity value was corrected accordingly.

A low-voltage alternating current was used to heat the Nichrome ribbons. The electrical circuit, shown in figure 4, was duplicated for each ribbon. The power dissipation in the heater ribbons was calculated from measured values of the current and resistance. The current was obtained by measuring the voltage drop across a resistor in series with the heater. The resistances of the heater and series resistor were measured with a double Kelvin bridge to within 1×10^{-5} ohm or 1 percent in the case of the smallest resistance. The temperature coefficient of resistance of Nichrome is small, and for the temperature range of these experiments, variation of the resistance of the heater was negligible.

FLOW SYSTEM AND TEST DUCT

The flow system used in the experiments is shown schematically in figure 5. The duct was constructed of 8-inch-nominal-diameter seamless steel pipe. Air from the room was pulled through the siren and into the duct by an exhauster facility. The flow rate was controlled by a large butterfly valve in conjunction with a smaller butter-

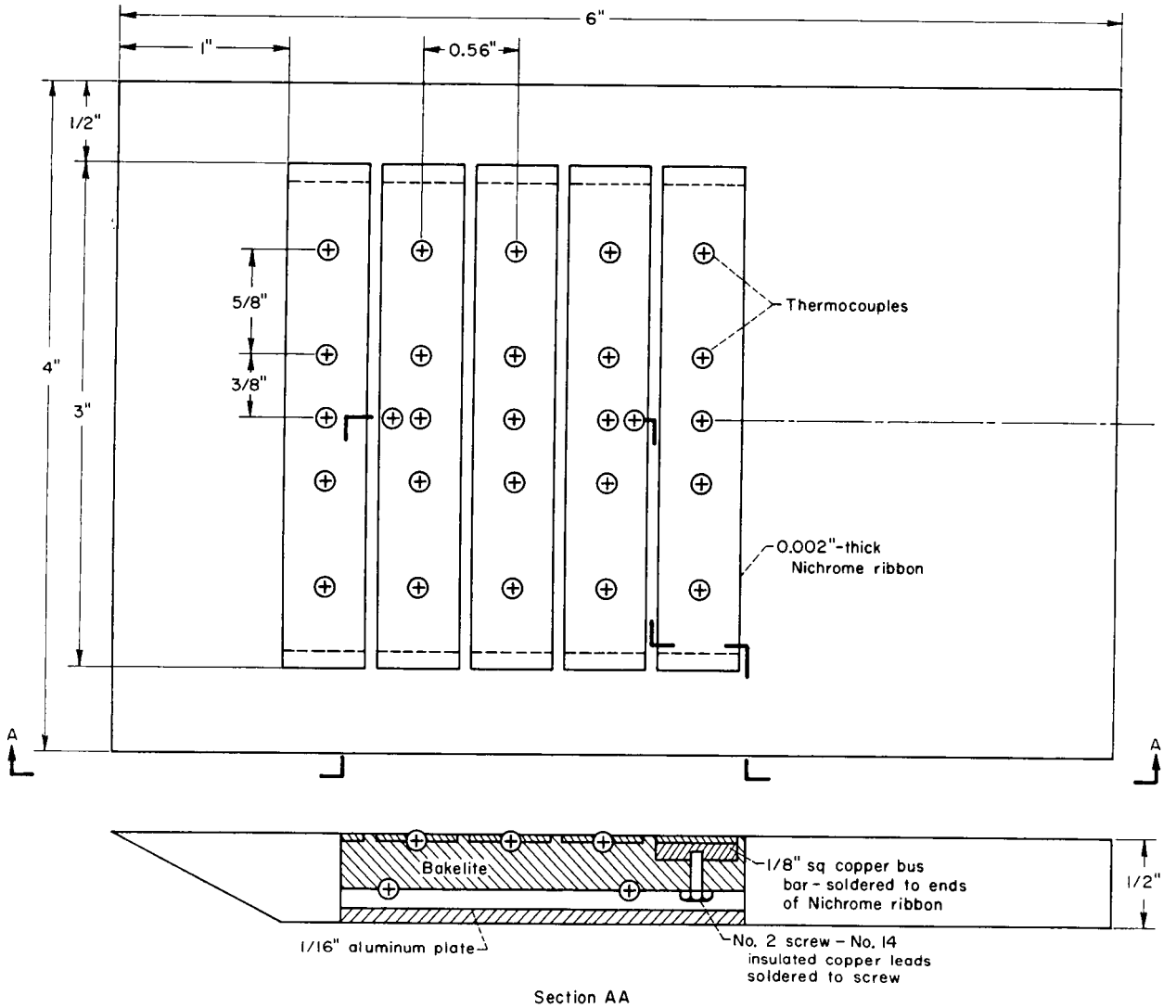

FIGURE 3.—Flat plate.

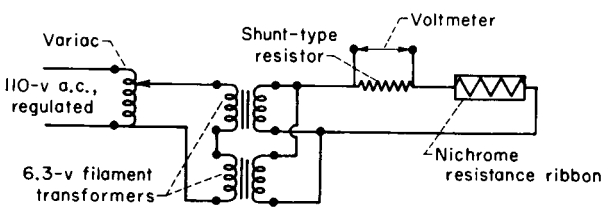

FIGURE 4.—Heater circuit.

fly valve located in the bypass line. A large commercial in-line muffler was installed just downstream of the test section in an effort to absorb the sound waves and thus prevent or minimize resonant conditions.

The test section was located about 5 feet from the siren. Optically flat glass windows were mounted in this section to permit optical studies of the boundary layer. The windows were 2 inches high and 6 inches long. Provision was also made at several locations along the duct for the introduction of instrumentation into the flow field.

The entire siren unit was enclosed in a wooden box having a volume of about 30 cubic feet. All the air entering the duct was filtered through several layers of fiber glass that were mounted over the entire end of the wooden enclosure. It was found that the filter was necessary to remove dirt and dust particles that interfered with the proper operation of the hot-wire anemometer. The enclosure also provided some reduction of the sound level in the room.

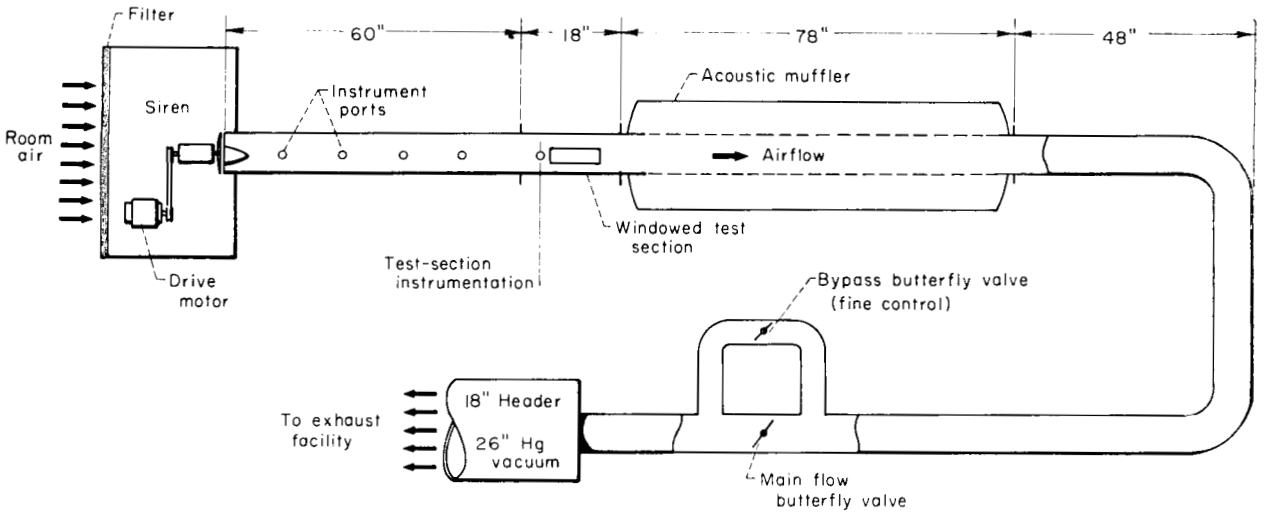

FIGURE 5.—Flow system.

HOT-WIRE ANEMOMETER AND CONDENSER MICROPHONE

The primary measurement of flow rate was made with a constant-temperature hot-wire anemometer (ref. 14). This instrument has received much use in the study of turbulent flows and seems ideally suited for measuring the large oscillating flows of this experiment. Since velocity, rather than pressure amplitude, was expected to exert the major influence on heat transfer, it seemed highly desirable to measure the velocity amplitude directly, rather than indirectly through pressures.

The wires used in the present work were tungsten, 0.0002 inch in diameter and 0.080 inch long. The probe was inserted into the flow field such that the axis of the wire was normal to the flow direction and the surface of the plate. The hot wire was calibrated against a pitot-static tube over the range of flow rates of interest both before and after each series of runs. This procedure was followed to ensure against possible shifts in the calibration curve such as are commonly caused by dirt accumulation on the wire.

An Altec-Lansing 21BR–220 condenser microphone was used to measure pressure oscillations. This microphone has a diaphragm 0.5 inch in diameter and a flat frequency response from about 10 to 10,000 cps. The output of the microphone was recorded on an oscilloscope and a true rms voltmeter. The microphone was mounted flush with the inside surface of the duct.

SCHLIEREN SYSTEM

Conventional system.—The schlieren system was of the twin-mirror type and could be adapted to high-speed photography. Light from a type BH6 mercury lamp in conjunction with a condensing lens was used to illuminate a slit 0.010 inch wide and 0.5 inch long that served as the source. The schlieren mirrors were spherical, were 6 inches in diameter, and had a 6-foot radius of curvature. With this system photographs of 0.1-second exposure were obtained in which the boundary-layer disturbances were time-averaged over several cycles of the flow oscillation. High-speed motion pictures were made with a 16-millimeter split-frame camera positioned behind the knife edge. The framing rate of the camera was 7000 to 8000 frames per second.

Modified system.—The schlieren system ordinarily indicates refractive index gradients by changes in the light intensity on the viewing screen or film. By means of the Thovert-Philpot-Svensson inclined slit method (ref. 15), the schlieren apparatus may be modified so that the gradients are indicated by a displacement of light rather than a change in intensity. The modified system is shown functionally in figure 6, where the schlieren mirrors have been replaced by lenses for clarity. A horizontal slit of 0.003-inch width, illuminated as described in the previous section, was used as the source. The knife edge was replaced by a wire of 0.02-inch diameter placed at a 45° angle from the horizontal and in the plane perpendicular to the optical axis of the schlieren system. In addition to the camera lens, a planoconvex cylindrical lens with its axis vertical was mounted in the imaging system. An

image of the source was projected onto the inclined wire, and an image of the test plate was projected onto the film plane but only in the vertical direction because of the cylindrical lens.

The cylindrical lens serves to focus the plane containing the inclined wire and the image of the light source onto the film plane, but only in the horizontal direction. If no refraction occurs, the light intercepted by the inclined wire appears on the film plane as a vertical line bounded on each side by light from the image of the source. In the presence of a refractive index gradient at a point on the model, a corresponding point on this line is displaced by a distance proportional to the gradient. Referring to figure 6, at the inclined wire,

$$\Delta y=\theta f=\Delta x \tan \alpha \tag{1}$$

where Δy is the vertical displacement of a fan of light rays, θ is the angle of refraction, f is the focal length of the schlieren lens, Δx is the horizontal displacement of the interception point of the wire and the fan of light rays, and α is the angle of inclination of the wire. At the film plane there results

$$D=m \Delta x \tag{2}$$

where m is the magnification factor of the lens system. The angle of refraction θ may be expressed as a function of the refractive index gradient and the distance of the disturbance along the optical path:

$$\theta=L\frac{dn}{dy} \tag{3}$$

where it is assumed that the gradient is perpendicular to the wave front and has a constant value along the optical path L. Combining these relations gives

$$\frac{dn}{dy}=\frac{D \tan \alpha}{fLm} \tag{4}$$

or

$$\frac{dn}{dy}=\left(\frac{\Delta y}{D}\right)_{cal}\frac{D}{fL} \tag{5}$$

where

$$\left(\frac{\Delta y}{D}\right)_{cal}=\frac{\tan \alpha}{m} \tag{6}$$

As indicated in equation (6), the system may be calibrated simply by moving the wire through a known distance Δy relative to the unrefracted light and measuring D in the film plane. This was accomplished by attaching the wire to the

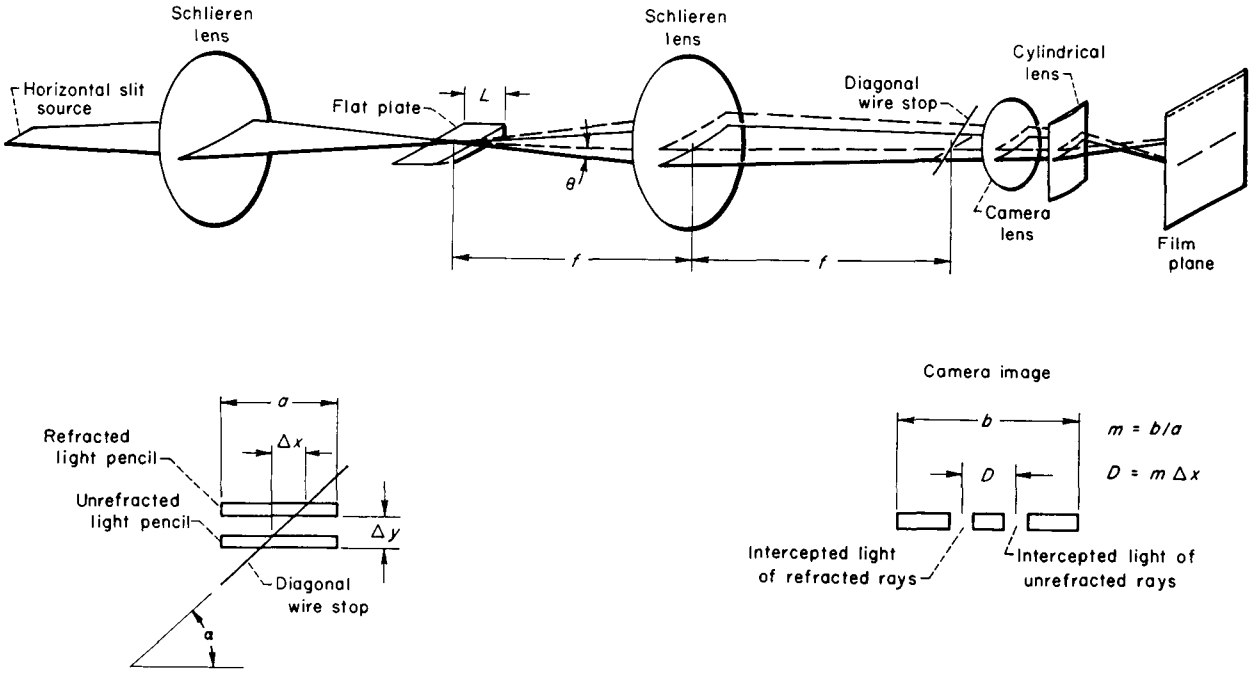

FIGURE 6.—Inclined-slit schlieren system.

micrometer screw feed of the knife-edge mounting. High-speed motion pictures were possible with this system also.

PROCEDURE

GENERAL

With the siren locked in the fully open position, a flow was established in the duct, and the power to each ribbon was adjusted until the temperature of all ribbons agreed within ±2 percent. Upon achieving this condition, the Variacs regulating the power to the ribbons were never changed so that all tests were conducted at the same heat-input rate.

A period of about 20 minutes, as determined by experience, was required at each flow rate to permit equilibrium to be reached. The thermocouples and power were then monitored for a 20-minute period with readings taken every 5 minutes. At the same time, pictures of the oscilloscope display of the hot-wire and microphone signals were taken. In this fashion, data points were obtained at each of a series of flow rates.

The same procedure was followed with oscillating flows. The desired oscillation frequency was obtained by adjusting the voltage to the siren motor while observing the Lissajous patterns on the oscilloscope. The Lissajous patterns were obtained by feeding the output of a calibrated audiofrequency generator into the x-axis and the microphone and hot wire each into the y-axis of a two-beam oscilloscope.

To evaluate the effects of frequency and amplitude individually on the heat-transfer coefficient, a frequency was selected and a series of points were taken at various amplitudes. Amplitude was varied by changing the spacing between the rotor and stator of the siren. The siren spacing was then fixed, and frequency was varied. For both cases a series of flow rates was used to evaluate the effect of mean flow rate.

REDUCTION OF DATA

Flow rate and pressure.—The microphone and hot-wire signals were displayed on the screen of a dual-beam oscilloscope and photographed on 35-millimeter film. It was not possible to rely on voltage-averaging meters to obtain the average flow rate and amplitude because of the nonlinear relation between flow rate and hot-wire voltage. Such methods are applicable only when the flow fluctuations about the mean are small. Therefore, instantaneous flow rates were computed at a number of times during a period of oscillation. In this way 10 to 16 cycles at each flow condition were averaged to obtain a curve representing one cycle of the oscillation. The time-averaged or mean flow was then computed according to the equation

$$\overline{\rho V}=\frac{1}{\lambda}\int_0^{\lambda}(\rho V)_i\,dt \tag{7}$$

where λ is the period of oscillation. The deviation of the flow from the mean value was characterized by the root-mean-square amplitude defined by the equation

$$(\rho V)_{rms}=\left\{\frac{1}{\lambda}\int_0^{\lambda}[(\rho V)_i-\overline{\rho V}]^2dt\right\}^{1/2} \tag{8}$$

Integration was performed graphically in both computations.

The microphone output voltage is a linear function of pressure so that root-mean-square pressure amplitudes were computed from the root-mean-square voltage indicated by a Ballantine True R.M.S. Voltmeter Model 320. This eliminated the need for the laborious graphical procedures that were required for flow rate determinations. The microphone was calibrated by means of a General Radio Company Type 1552-B Sound-Level Calibrator, which delivered a 121-decibel (re. 10^{-16} w/sq cm) pressure level at 400 cps to the microphone.

Heat-transfer coefficient.—The heat-transfer coefficient to the airstream was computed from the measured power input to the ribbons corrected for measured conduction losses and the temperature difference between the ribbons and the airstream. Uniform heat generation in the ribbons was assumed. At equilibrium, the heat balance is

$$q_{gen}=q_{conv}+q_{cond}+q_{rad} \tag{9}$$

where the terms refer to the various mechanisms by which the heat may be dissipated. The radiation heat loss q_{rad} was negligible for the temperature involved, even when blackbody emissivity was assumed.

Conduction losses were considered along all three axes of the plate. In the direction of flow, the plate was essentially isothermal so that heat flow in this direction was negligible. In this connection, the first and last ribbons were guard

heaters, and the conduction losses from them to the unheated portions of the plate were not considered.

In the lateral direction, across the surface of the plate, the heat conduction loss was calculated from the temperature difference measured by thermocouples located at a known distance from the center thermocouple. This loss amounted to less than 1 percent of the heat generated.

The major heat loss, amounting to about 10 percent of the heat generated, occurred by conduction to the lower surface of the plate. This loss was computed, as in the previous case, from direct measurement of the temperature drop through the body of the plate.

With the heat loss correction accounted for, the convective heat-transfer rate was calculated by difference according to equation (9). Finally, the convective heat-transfer coefficient given by

$$h=\frac{q_{conv}}{A\,\Delta T}\ \frac{\text{Btu}}{(\text{hr})(\text{sq ft})(^\circ\text{F})} \tag{10}$$

was calculated, where A is the area of the exposed surface of the ribbon and ΔT was measured between the ribbon and the airstream. All values of ΔT were obtained from measurements with a Rubicon potentiometer and an external moving-light beam galvanometer to the nearest slide wire division or within about 0.35° F.

The heat-transfer coefficient was expressed in dimensionless form by the Nusselt number

$$Nu_x=\frac{hx}{k} \tag{11}$$

where x is the distance from the leading edge of the plate to the center of a ribbon and k is the thermal conductivity of air.

EXPERIMENTAL RESULTS

REFERENCE FLOW CHARACTERISTICS

Velocity profile in duct.—The inlet configuration of the duct was somewhat unusual because of the siren. It was desired that the reference flow condition should duplicate the oscillating flow as closely as possible with the exception of the oscillations. Therefore, the siren was left on the duct in establishing the reference flow, and the rotor was locked in place with the ports fully open. The velocity profiles across the duct for the reference flow were flat within about ±5 percent up to 1 inch from the duct wall. These profiles were measured with a pitot-static tube. A slight minimum in the profiles occurred at the centerline of the duct because of the "shadow" cast by the hub of the siren.

Turbulence properties.—The major distinguishing feature observed for the reference flow was its intensity of turbulence. Over the range of flow rates studied, the free-stream turbulence intensity ranged from 9 to 10 percent. This was considerably higher than generally encountered in wind tunnels; however, it was not unexpected because the siren ports could function as turbulence generators much like a grid or coarse mesh screen. To examine the reference flow further, the frequency spectrum of the turbulence was determined. The hot-wire signal was fed into a harmonic analyzer having an effective bandwidth of 4.5 cps and a frequency range of 20 to 16,000 cps. The resulting energy-frequency distribution is shown in figure 7. For comparison, the spectrum from a tunnel having the usual flow-generated turbulence is also shown (ref. 16). The free-stream velocity associated with the comparison curve is 45.5 feet per second, which is near the midpoint of the velocity range covered in the present experiments. The two curves are quite similar, the only difference being a possible shift of the turbulent energy to a somewhat lower frequency range in the present work. The additional energy in the low-frequency range may be explained by the relatively large size of the "grid-like structure" of the siren. Because of its size it should be expected that the eddies from the siren are large and are shed at low frequency. Such is the case in the analogous situation of vortex shedding from a cylinder.

OSCILLATING FLOW CHARACTERISTICS

As mentioned previously, the duct incorporated a large acoustic muffler to obtain a traveling wave system rather than a resonant system. As will be shown, the resulting wave system shows characteristics of both systems but appears to be more closely related to the traveling wave system. In figure 8, the instantaneous time variation of pressure and flow rate is represented at several frequencies by the oscilloscope traces of the microphone and hot-wire signals. These data were obtained at the test section in the free stream.

A considerable amount of distortion was observed in the waveforms as a consequence of the

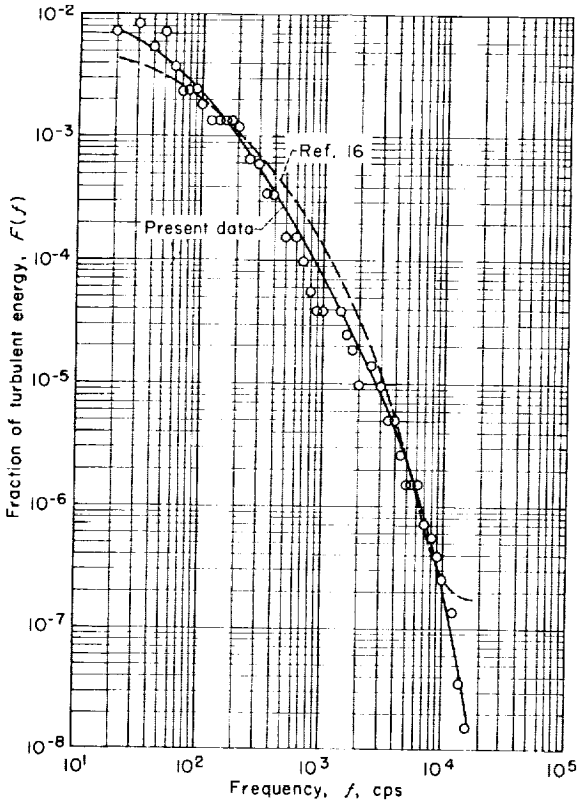

FIGURE 7.- Turbulent energy-frequency spectrum.

high sound-pressure levels. An approximate harmonic analysis of the waveform at a low and a high frequency indicated that from about 4 to 12 terms of the complete Fourier sine-cosine series were needed to approximate the waveform. The larger number of terms applies to the higher frequency. It was also observed that flow reversal occurred in the free stream at some frequencies. The region of flow reversal corresponds to the small peak around the minimum in the hot-wire signals obtained at 46 and 148 cps. The positive direction indicated by the hot-wire signal is due to the fact that the wire does not sense flow direction, and thus the signal is rectified. On comparing the pressure and flow rate signals it was observed that pressure varied in phase with respect to the flow rate. That is, the time of the pressure minimum occurred at the time of minimum flow rate.

It was found that frequency was not continuously variable except at flow rates considerably less than those actually used in the experiment. The reason for this behavior was probably due to some mode of resonant coupling between the duct and the siren. The siren was found to lock-in on certain frequencies, which were used in the experi-

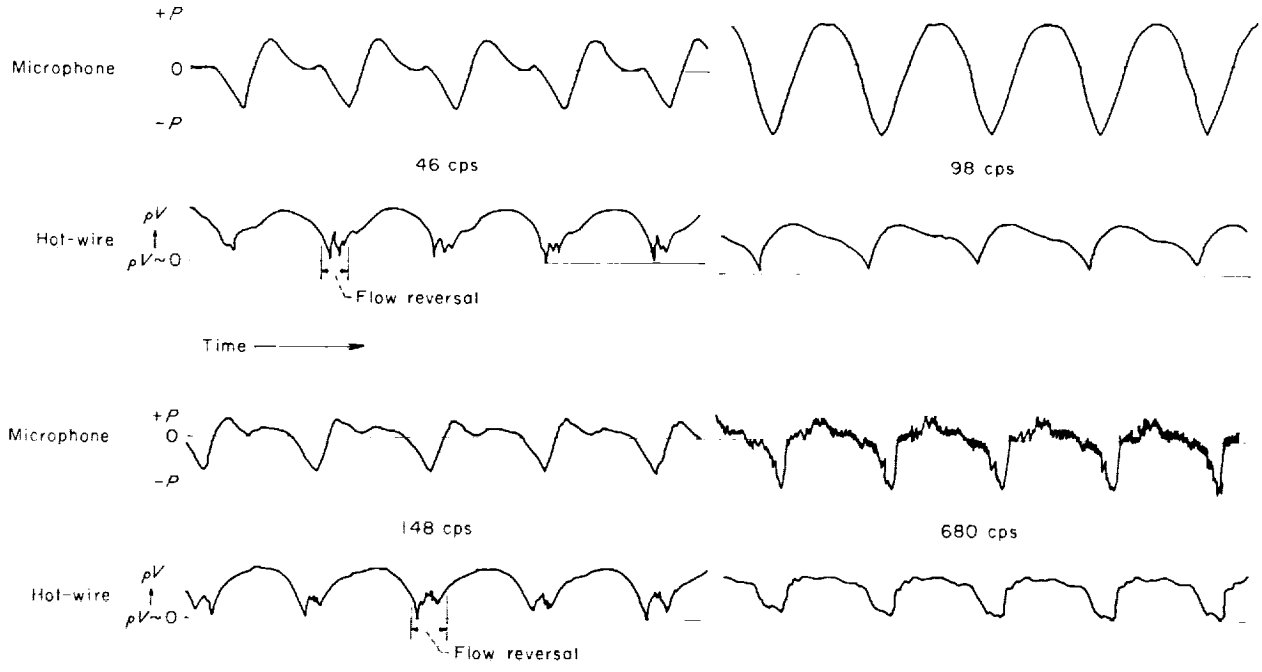

FIGURE 8.—Oscillograph traces of microphone and hot-wire signals.

ment. In order to evaluate the degree of resonance present, it was necessary to measure the standing-wave ratio of the sound field in the duct.

The standing-wave ratio was not measured exactly because of the difficulty of traversing the duct axially with the microphone; however, it was approximated by locating the microphone at several stations along the duct. From these data, approximate curves of root-mean-square pressure amplitude against distance were obtained as shown in figure 9. The data indicate that a moderate amount of resonance was present; the maximum value of the standing-wave ratio was about 2.5 and occurred at 98 cps. It may be concluded that each frequency used in the experiments corresponded closely to a resonant frequency of the duct. The fundamental frequency of the duct was 17 cps, corresponding to that of a 34-foot-long pipe closed at both ends. This distance corresponds to that from the siren to the butterfly control valve, which constituted a closed end because the pressure ratio across the valve exceeded the critical value, and the flow through the valve was therefore sonic or choked. The frequencies used corresponded to harmonics of the duct ranging from the second to the fortieth.

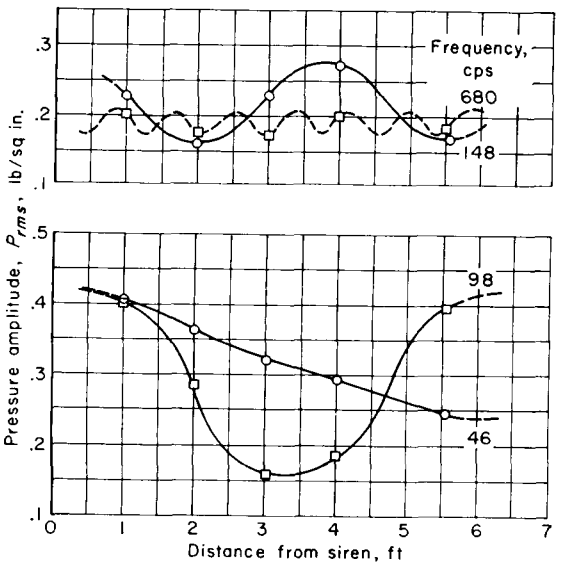

FIGURE 9.—Variation of root-mean-square pressure amplitude showing nodes and antinodes.

At a given spacing between the rotor and stator of the siren, the pressure and velocity or flow rate amplitudes were functions of the mean flow rate. This dependence is shown in figure 10 where root-mean-square pressure amplitude and root-mean-square flow amplitude are plotted against mean flow rate for several frequencies. These data were taken at the test station. The variation of the proportionality constant reflects the changing position of the test section with respect to nodes and antinodes as frequency was changed.

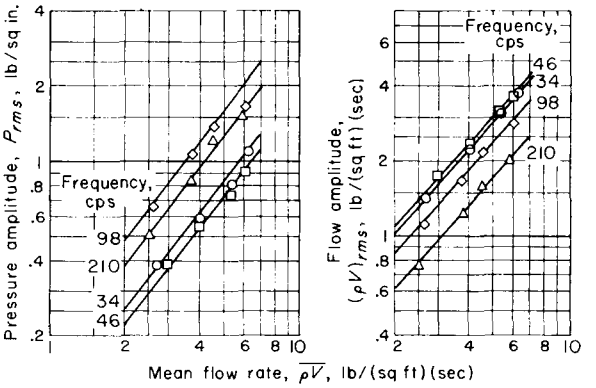

FIGURE 10.—Variation of amplitude parameters with mean flow rate.

The frequency dependence indicated by figure 10 is illustrated in figure 11 where the two amplitude parameters are plotted against frequency at an approximately constant value of the mean flow rate. The maximums and minimums shown indicate, as previously stated, the relation of the test section to nodes and antinodes in the wave. It was observed that the magnitude of the swings in amplitude diminished as frequency was increased and also that amplitude, in general, decreased. This is in accord with general knowledge of the frequency behavior of constant-energy sound.

From the foregoing discussion it was concluded that the wave system set up in the duct was largely a traveling wave with a small standing-wave component. The largest value of the standing-wave ratio observed was approximately 2.5 and occurred at 98 cps. The wave was also essentially plane-fronted. This was demonstrated by locating two hot wires at the same axial station along the duct but at different radial positions and observing that the two signals were superimposable.

HEAT TRANSFER WITHOUT SOUND

The Nusselt-Reynolds number relation found without sound is shown in figure 12 for stations 2 and 3. The length parameter in both dimension-

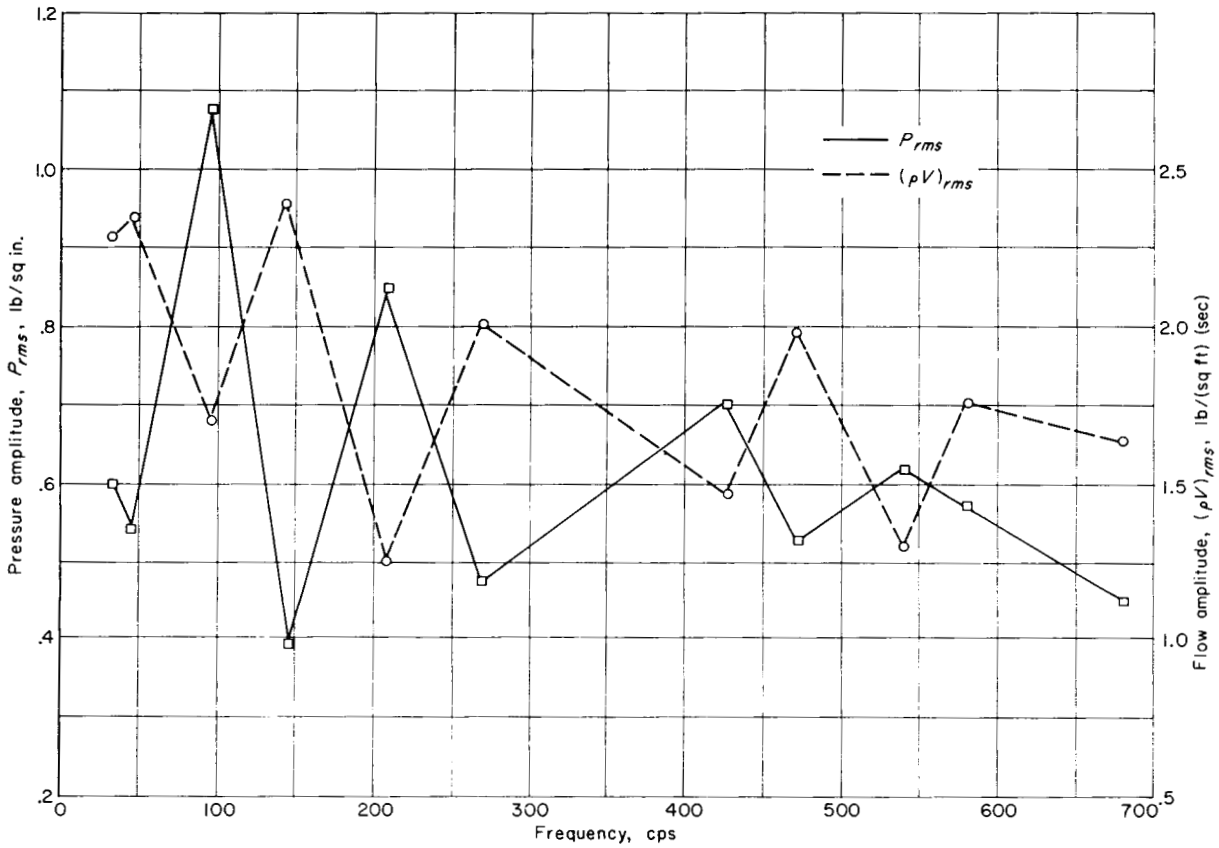

FIGURE 11.—Variation of amplitude parameters with frequency. $\overline{\rho V} \sim 3.8$.

less numbers corresponds to the x-distance measured from the plate leading edge. The tendency of the data points in figure 12 to assume a horizontal grouping pattern is a consequence of the way the data were obtained and reflects the lesser degree of reproducibility of the velocity measurement compared with the temperature measurement. The data were taken before and after each series of experiments with sound to provide a check on the behavior of the plate. The data at each station were fitted by the method of least squares to the general equation of the form:

$$Nu_x = BRe_x^M \tag{12}$$

The standard deviation in Nusselt number of the resulting expression was ± 12, corresponding to a probable error of about 3.5 percent based on the average Nusselt number. The Prandtl number was treated as a constant in this work because of the small variation in temperature. The maximum variation in the Prandtl number that could occur was less than 0.1 percent.

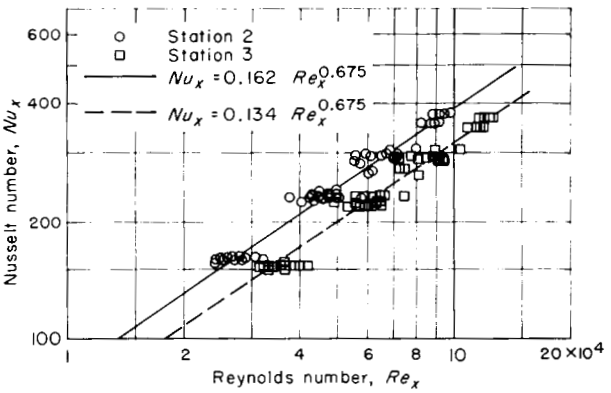

FIGURE 12.—Heat transfer without sound.

HEAT TRANSFER WITH SOUND

The data obtained by varying the rotor-stator spacing at a constant frequency of 46 cps are tabulated in table I and plotted in figure 13.

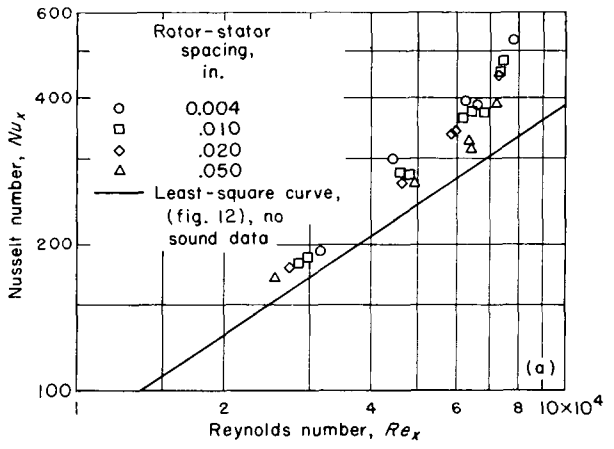

(a) Station 2.

FIGURE 13.—Heat transfer at 46 cps for various rotor-stator spacings.

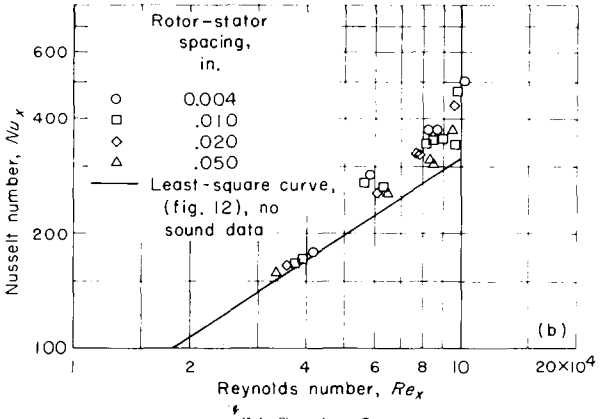

(b) Station 3.

FIGURE 13.—Concluded. Heat transfer at 46 cps for various rotor-stator spacings.

The least-square curves obtained for the no-sound condition are also shown in figure 13 for comparison. With sound, the Reynolds number was based on the time-averaged flow rate. The magnitude of the increase in Nusselt number with sound varied from about 3 percent at low Reynolds numbers to 60 percent at the highest Reynolds numbers. In table II are tabulated the data obtained at various frequencies and fixed rotor-stator spacing. The Nusselt-Reynolds number plot of these data closely resembles that shown in figure 13. The variation of Nusselt number with frequency is shown in figure 14 at an approximately constant value of the Reynolds number. Only one Reynolds number value is shown, but the results are typical of those at other Reynolds numbers. A comparison of figure 14 with figure 11 shows that the variation of Nusselt number with frequency follows the same general trend as does the root-mean-square velocity amplitude with the exception of one or two frequencies.

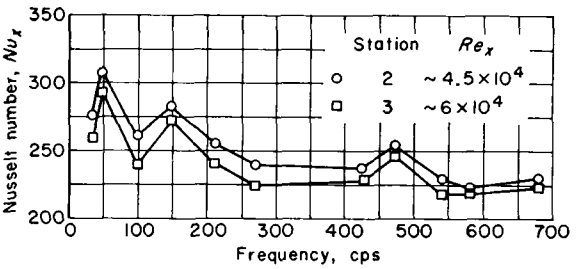

FIGURE 14.—Variation of Nusselt number with frequency.

CORRELATION OF DATA

The Nusselt numbers found in these experiments were larger than those predicted by the usual heat-transfer equations, even without sound. The reason for this result, in the absence of sound, is believed to be the high turbulence intensity (10 percent) present compared with the 2 to 3 percent or less turbulence intensity generally encountered. Also, the data without sound did not follow the usual Reynolds number power dependency. Any correlation of the data then should reflect these observations. It was therefore decided to attempt to correlate the data by a relation of the form:

$$Nu_x = f_1(\epsilon) Re_x^{f_2(\epsilon)} \tag{13}$$

where ϵ is the turbulence intensity in the case of the reference flow. With sound, ϵ becomes the ratio of the root-mean-square velocity or flow rate to the time-averaged flow rate $(\rho V)_{rms}/\overline{\rho V}$, which is analogous to the turbulence intensity. The Reynolds number was based on the time-averaged flow rate. As a lower limit, when ϵ approaches zero, it was assumed that the relation should reduce to the usual expression (ref. 17) for heat transfer in laminar flow given by

$$Nu_x = 0.332\, Pr^{1/3} Re_x^{1/2} \left[1 - \left(\frac{x_L}{x}\right)^{3/4}\right]^{-1/3} \tag{14}$$

where x_L is the unheated starting length on the plate (the distance from the leading edge of the plate to the first heater) and x is the distance from the leading edge to the point where heat transfer is measured. The term in brackets is a correction

factor to account for the delayed start of the thermal boundary layer compared with the hydrodynamic boundary layer. For a Prandtl number of 0.71 this equation reduces to

$$Nu_x = 0.415\ Re_x^{1/2} \quad \text{(Station 2)} \qquad (15)$$

and

$$Nu_x = 0.379\ Re_x^{1/2} \quad \text{(Station 3)} \qquad (16)$$

With these equations, the correlation expression becomes

$$Nu_x = [f_1(\epsilon)]Re_x^{0.5+f_2(\epsilon)} \qquad (17)$$

where $f_1(\epsilon)$ also depends upon the station, and the functions $f_1(\epsilon), f_2(\epsilon)$ are to be determined from the experimental data.

The functions $f_1(\epsilon)$ and $f_2(\epsilon)$ are shown in figures 15 and 16, respectively. The former varies inversely with ϵ, while the latter varies directly with ϵ. The function $f_1(\epsilon)$ is given within about 10 percent by the relations:

$$f_1(\epsilon) = 0.415\ (10^{-2.6\epsilon^{0.72}}) \quad \text{(Station 2)} \qquad (18)$$

and

$$f_1(\epsilon) = 0.379\ (10^{-2.75\epsilon^{0.72}}) \quad \text{(Station 3)} \qquad (19)$$

As indicated by the variation in slope, there was a small additional dependency upon x-distance or station not accounted for in the starting-length correction factor. The function $f_2(\epsilon)$ is given by the following relation for both stations:

$$f_2(\epsilon) = 0.65\epsilon^{0.57} \qquad (20)$$

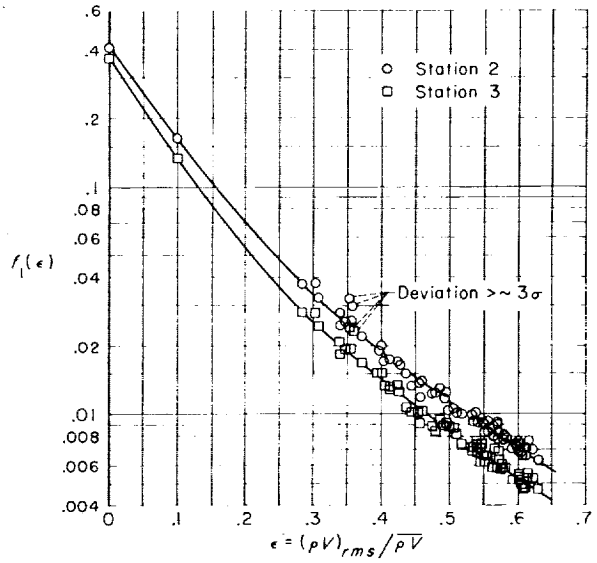

FIGURE 15. Coefficients of correlation expression.

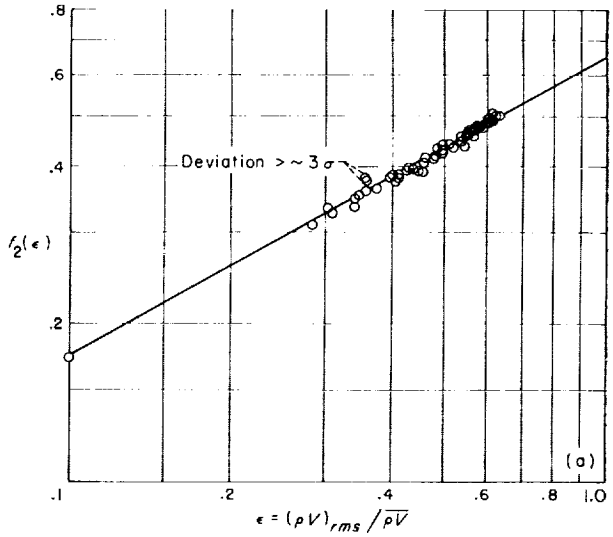

(a) Station 2.

FIGURE 16.—Exponents of correlation expression.

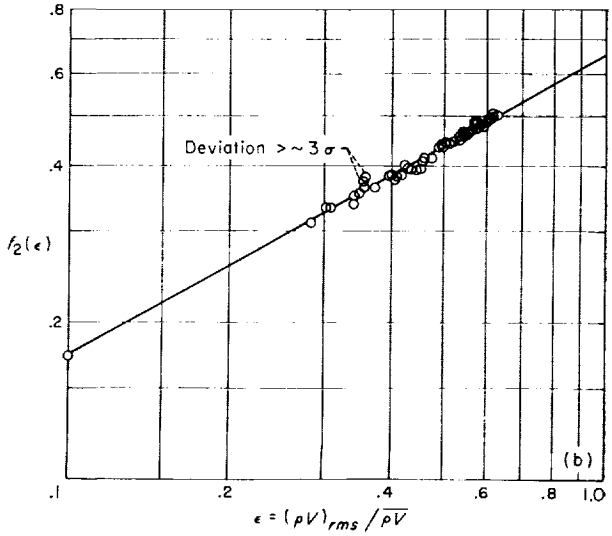

(b) Station 3.

FIGURE 16.—Concluded. Exponents of correlation expression.

With these relations for $f_1(\epsilon)$ and $f_2(\epsilon)$, the expression correlating both the data with and without sound may be written

$$Nu_x = 0.415\ (10^{-2.6\epsilon^{0.72}})\ Re_x^{0.5+0.65\epsilon^{0.57}}$$

(Station 2) (21)

and

$$Nu_x = 0.379\ (10^{-2.75\epsilon^{0.72}})\ Re_x^{0.5+0.65\epsilon^{0.57}}$$

(Station 3) (22)

In general form the expression may be written as

$$Nu_x = 0.332\, Pr^{1/3}\left[1-\left(\frac{x_L}{x}\right)^{3/4}\right]^{-1/3} \times 10^{g(x_L/x)(\epsilon)^{0.72}} Re_x^{0.5+0.65\epsilon^{0.57}} \quad (23)$$

The results of the correlation are shown in figure 17 where the experimental Nusselt number with sound is plotted against the Nusselt number calculated from the empirical expressions (eqs. (21) and (22)) for both stations 2 and 3. Excluding the two pair of data points indicated, the standard deviation of the correlation was ± 21 in terms of the Nusselt number. The corresponding probable error was 4.8 percent, or 1.3 percent greater than the value obtained for the reference flow data. The increase may be accounted for, in part, by the error introduced by the graphical computation of $(\rho V)_{rms}$. It may be concluded that the heat transfer does not depend on frequency over the range which frequency was varied.

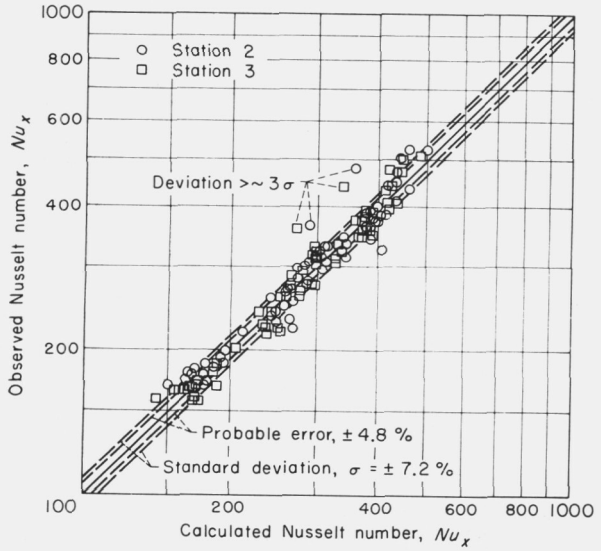

FIGURE 17.—Comisonpar of experimental and calculated Nusselt numbers for oscillating flow.

SCHLIEREN STUDIES

Experiments with conventional schlieren.—Figure 18 shows representative time-averaged schlieren photographs of the thermal boundary layer at a magnification of 3. The boundary layer shown by the schlieren techniques was detected only in the presence of heating. Refer-

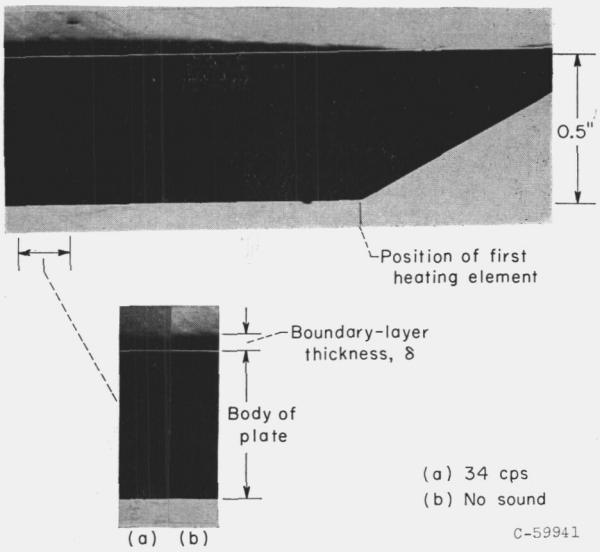

FIGURE 18.—Time-averaged schlieren boundary-layer photographs.

ences to boundary-layer measurements by the schlieren method, therefore, refer to the thermal boundary layer. By comparing the photographs at the two flow conditions, it may be seen that the time-averaged boundary layer with sound is thinner than that without sound. With the aid of a microdensitometer, comparative values of the boundary-layer thickness at a constant value of the temperature gradient (i.e., the distance from the plate surface at which the temperature gradient reached a prescribed value) were measured at the different frequencies. The data so obtained are shown in figure 19 where the ratio δ_o/δ_f of the thickness without sound to that with sound is plotted against frequency. The data indicate that the flow oscillations produce a net decrease in the thickness of the boundary layer.

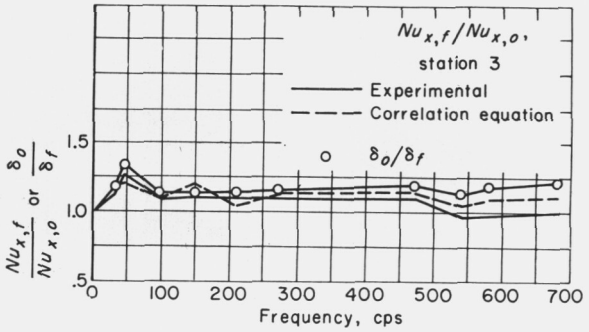

FIGURE 19.—Comparison of variation of boundary-layer thickness and Nusselt number with frequency.

For comparison, the ratio $Nu_{x,f}/Nu_{x,o}$ of the Nusselt number with sound to that without sound is also shown. The heat-transfer data are those of figure 14 for station 3, and curves for both the experimental Nusselt number and the value calculated by the correlation equation are shown. In general, the two ratios, δ_o/δ_f and $Nu_{x,f}/Nu_{x,o}$, follow the same trend with frequency. Thus, in agreement with theory, these results show that the Nusselt number varied inversely with boundary-layer thickness. The generally lower values of the Nusselt number ratio compared with the values of the boundary-layer ratio may be accounted for by the fact that the former were obtained at a somewhat lower value of the mean flow rate. The maximum difference in the two parameters was about twice the probable error of the heat-transfer correlation.

In figure 20 are representative sequences from high-speed films of the thermal boundary layer at several flow conditions. The object in the photographs below the leading edge of the plate is a lens that was taped to the outside surface of the lower window and was used for focusing purposes. The boundary layer in the reference flow is shown in figure 20(a). The layer is rather irregular and wispy in appearance. It appears to be broken up randomly into small tufts. At the outer edge of the layer, small fragments of these tufts were rapidly dissipated by the free-stream flow. In gross appearance, the layer tends to remain unchanged with time.

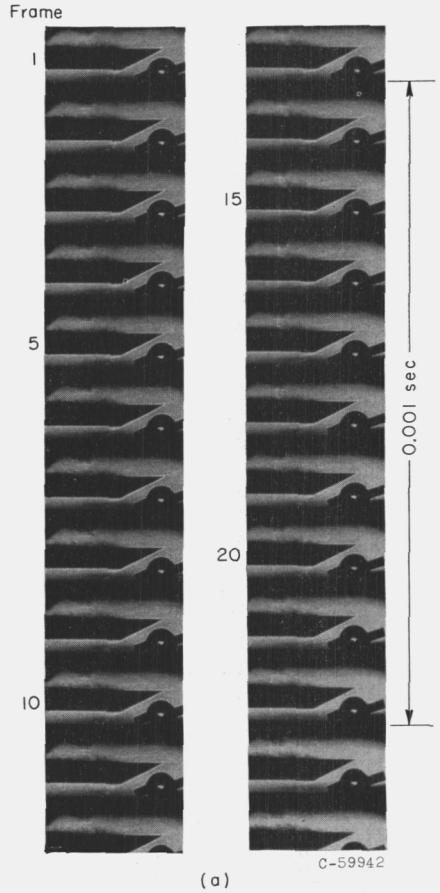

(a) Reference flow.

FIGURE 20.—High-speed schlieren photographs of boundary layer.

Figure 20(b) shows a complete cycle of the boundary-layer flow at 148 cps. In detailed appearance, the layer does not seem to differ appreciably from that in the reference flow. However, there was a large variation in appearance with time; with sound, flow reversal was observed in the boundary layer at all frequencies. Flow reversal is shown in frames 1 to 10 of figure 20(b), in which the layer grows outward and in the upstream direction on the plate. During reversal, fragments of the layer were dispersed in the free stream near the leading edge of the plate. By frame 17 the flow has started to accelerate in the downstream direction, and the thick layer formed during reversal is swept along with it. In place of the thick layer, a very thin layer was formed that is completely developed by frame 36 and appears to remain stable to about frame 48. As the flow decelerates, this new layer slowly grows in thickness to frame 60 where flow reversal begins to appear again.

A similar sequence is shown in figure 20(c) at 98 cps, where flow reversal occurred in frames 1 to 15. The flow has started to accelerate in the downstream direction at about frame 24 and continues through frame 36. The 36 frames shown constitute about one-third of a complete cycle.

Experiments with modified schlieren.—Because of experimental difficulty, discussed in the following paragraph, only a few tests were made with the modified schlieren system, and these were made on an earlier model of the plate that had an elliptical leading edge. The results obtained will be discussed, however, for they illustrate some interesting facts. Referring to the sketch in figure 21, the magnitude of the displacement of the image of the wire is proportional to the refractive index gradient or temperature gradient

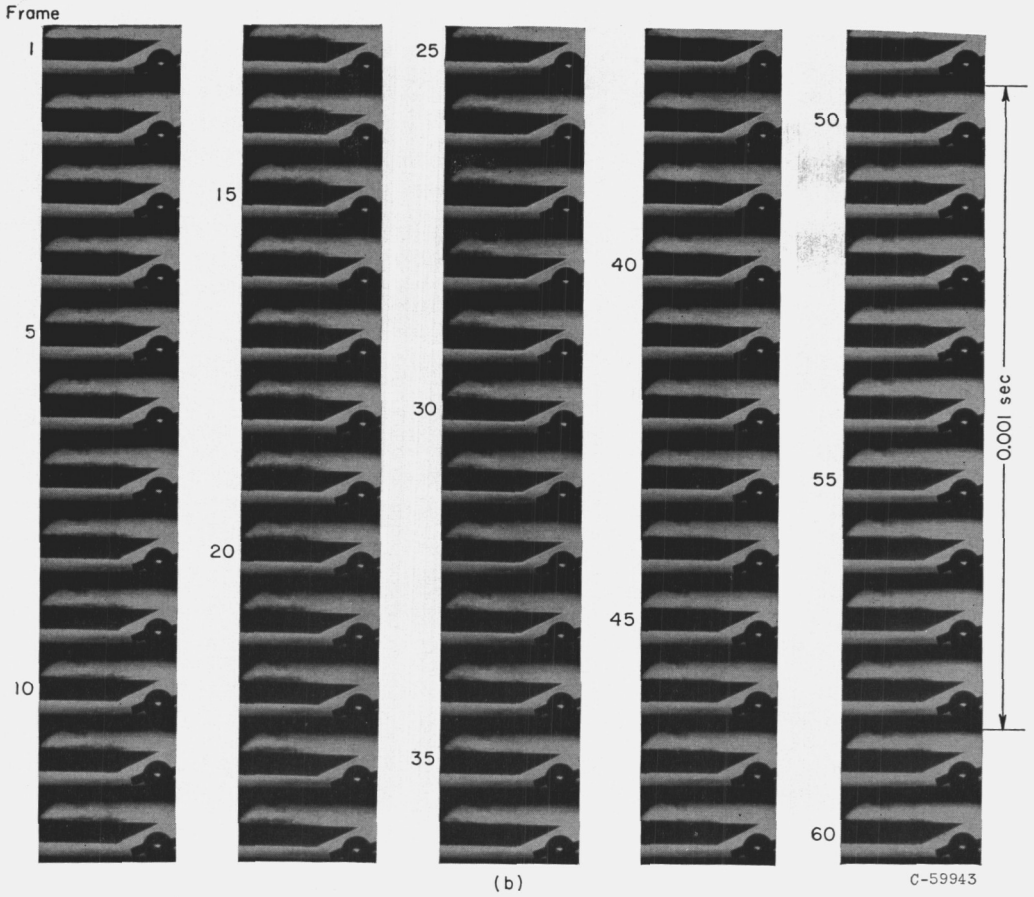

(b) 148-Cps oscillation.

FIGURE 20.—Continued. High-speed schlieren photographs of boundary layer.

at the surface of the plate. The distance from the plate surface to the point where displacement first occurs is proportional to the boundary-layer thickness. Thus, the curve traced by the image of the wire is essentially that of the temperature gradient against distance through the boundary layer. The direction of the temperature gradient determines the direction of displacement of the image.

When this technique was applied to the study of the reference-flow boundary layer, good agreement was obtained at low flow rates, between the values of $(dT/dy)_{y=0}$ measured by the schlieren method and those calculated from the measured heat-transfer rate. The former value was obtained by extrapolating the temperature gradient to the value at the wall, while the latter was computed from the measured heat-transfer rate according to the relation $\frac{q_{conv}}{A}=-k(dT/dy)_{y=0}$. However, as the flow rate was increased, the agreement became progressively poorer so that, at the highest flow rate, the schlieren value was about one-third of the calculated value. The reason for this behavior was that, as the flow rate was increased, the boundary-layer thickness decreased, and the temperature gradient increased to such an extent that it was impossible to resolve the trace of the image of the wire on the film. Optical diffraction at the wire also interfered with resolution of the trace as did that at the surface of the plate.

In figure 21 are shown high-speed photographs obtained with the modified schlieren system for a complete cycle of the oscillation at 148 cps and a mean flow rate of 0.5 pound per square foot per second. Close examination of these photographs reveals that the temperature gradient at the wall reaches a minimum value at about frame 20. At the same time the boundary layer reaches its maximum thickness. These results are shown

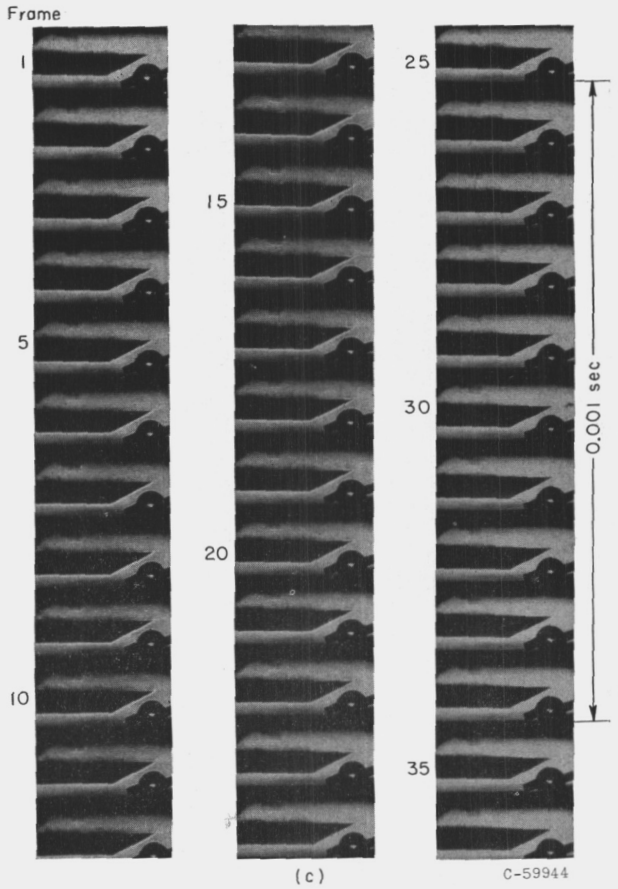

(c) 98-Cps oscillation.

FIGURE 20.—Concluded. High-speed schlieren photographs of boundary layer.

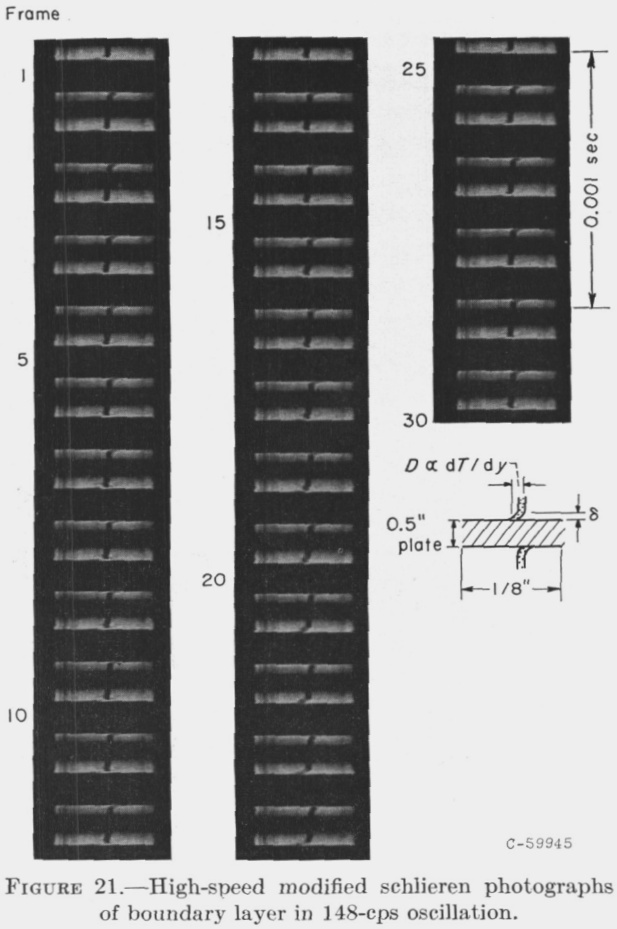

FIGURE 21.—High-speed modified schlieren photographs of boundary layer in 148-cps oscillation.

in figure 22 where values of dT/dy at various y-distances and the boundary-layer thickness are plotted over a cycle of the oscillation. The values were obtained from smoothed plots of dT/dy against y-distance. The integrated average value of $(dT/dy)_{y=o}$ at this low flow rate was in good agreement with that calculated from the heat-transfer rate, the difference being about 5 percent.

The theoretical relations among the various parameters are given by the following equations:

$$\frac{q_{conv}}{A}=-k\left(\frac{dT}{dy}\right)_{y=0}=h\,\Delta T=\frac{k}{\delta}\Delta T' \qquad (24)$$

Since $(dT/dy)_{y=0}$ was observed to vary over the period of an oscillation, it follows that the heat-transfer rate q_{conv} also will vary. The data show also that δ, the boundary-layer thickness, varied with time. From equation (24) the temperature difference $\Delta T'$ is given by

$$\Delta T'=\left(\frac{dT}{dy}\right)_{y=0}\delta \qquad (25)$$

Values of $\Delta T'$, computed from equation (25) and plotted in figure 22, appear to be essentially constant. This may be seen more clearly in figure 23, where the values of $\Delta T'$ are plotted against δ. The band defining the points is horizontal and thus establishes the relative constancy of $\Delta T'$. Figure 23 also shows the variation of $(dT/dy)_{y=0}$ with $1/\delta$. The data are linear within the 10-percent scatter shown and thus agree with equation (25). The average value of $\Delta T'$ given by the slope was about 55° F, while the experimental value indicated by the thermocouple measurement was 27.2° F. This indicates only that the temperature gradient was not linear through the boundary layer as assumed by equation (25).

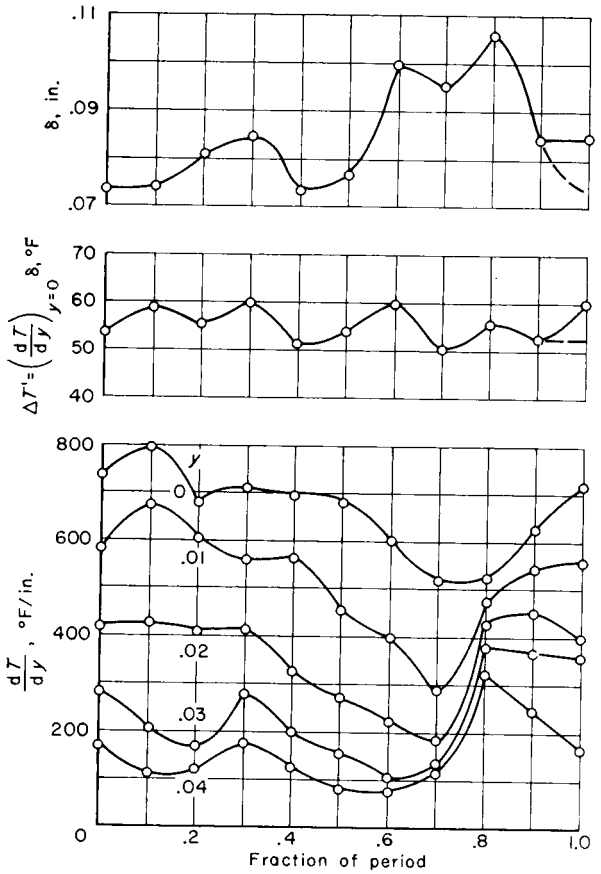

FIGURE 22.—Variation of δ, $\Delta T'$, and dT/dy during oscillations.

The results of the schlieren studies may be summarized as follows:

(1) At a given flow condition, ΔT was time-invariant. The parameters q_{conv}, h, δ, and $(dT/dy)_{y=0}$ varied with time.

(2) For various flow conditions, the time-averaged values of q_{conv} and therefore $(dT/dy)_{y=0}$ were constant if small changes in the conduction heat loss are neglected. The reason for this result is that the tests were conducted with a constant time-averaged power input to the ribbons. The time-averaged values of the parameters h, ΔT, and the temperature profile, or δ, all varied with flow conditions.

DISCUSSION OF RESULTS

All the flows studied in these experiments were characterized by random perturbations or periodic oscillations about the mean or time-averaged flow rate. The magnitude of the deviation from the mean flow rate was given by the parameter

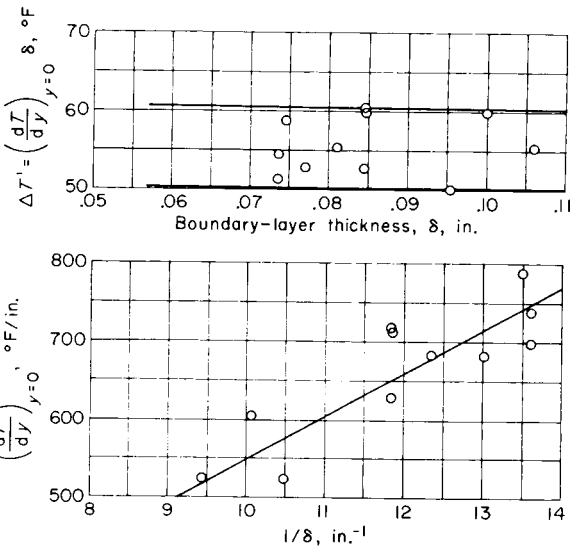

FIGURE 23.—Variation of instantaneous temperature parameters with instantaneous boundary-layer thickness.

$\epsilon \equiv (\rho V)_{rms}/\overline{\rho V}$. For both kinds of flow, periodic and turbulent, an increase in the heat-transfer coefficient was observed, compared with that predicted from the mean flow rate according to accepted expressions in the literature for the flat plate.

With the Reynolds number in oscillating flow based on the time-averaged flow rate, increases of as much as 65 percent in the Nusselt number were observed during oscillations. For a similar comparison based on the assumption of quasi-steady heat transfer, the increase was still larger. This may be readily seen from the relations defining the two processes for averaging the flow rate. They are given by

$$\left[\frac{1}{\lambda}\int_0^{\lambda} (\rho V)_i \, dt\right]^n \geq \frac{1}{\lambda}\int_0^{\lambda} (\rho V)_i^n \, dt \text{ for } n \gtrless 1 \quad (26)$$

where $(\rho V)_i$ is the instantaneous flow rate and the left and right terms are the time-averaged and quasi-steady values, respectively. The value of n describes the dependence of the Nusselt number on flow rate and usually has the values 0.5 and 0.8 for laminar and turbulent flows, respectively.

For the present data, the value of n obtained in the reference flow was 0.675, and this value was used in the quasi-steady flow-averaging computation. The quasi-steady Reynolds number was about 8 percent less than the corresponding linear time-averaged Reynolds number. Comparison of the Nusselt number with oscillations

with the reference Nusselt number corresponding to the quasi-steady Reynolds number showed that the increase with oscillations was as much as 74 percent.

A comparison of the experimental data with the various flow parameters revealed that the Nusselt number varied directly with the amplitude parameter ϵ at a constant value of the Reynolds number. It was found that the data for both kinds of flow could be correlated by an expression of the form

$$Nu_x = f_1(\epsilon) Re_x^{f_2(\epsilon)}$$

where both the coefficient and exponent were functions of ϵ. Thus, there was no independent effect on the heat-transfer rate of either pressure amplitude or oscillation frequency that could not be explained by the root-mean-square flow amplitude.

From the schlieren studies, it may be concluded that the temperature gradient or boundary-layer thickness was variable with time and also that the time-averaged values of these properties were influenced by the flow parameters to produce the heat-transfer results described by the correlation expression. The schlieren data also showed that flow reversal occurred in the boundary layer during a portion of each cycle. In a similar study of the flat plate in oscillating flow, it was found that the oscillation amplitude had to exceed a critical value in order to increase the heat-transfer rate (ref. 18). It was thought that this critical amplitude corresponded to that necessary to produce flow reversal.

The most likely explanation for these results appears to be the interaction of the flow and temperature fields through the mechanism of turbulence. The reasons for this assumption are: (1) The correlation expression fitted the present experimental data both for periodic flows and turbulent flows; (2) the structure of the boundary layer was similar in appearance in the two cases; and (3) the spectrum of turbulent energy measured for the reference flow revealed that virtually all this energy occurred in the same frequency range over which the oscillation frequency was varied. The similarity of turbulent flows and oscillating flows with regard to their effect on the heat-transfer process has been hypothesized in reference 4.

An expression for the Nusselt-Reynolds number relation in fully developed turbulent flow has been obtained in reference 19. The relation was derived from the expression previously obtained for the velocity profile in fully developed turbulent pipe flow in which the eddy diffusivity was evaluated (ref. 20). This expression does not predict the effect of turbulence intensity per se; however, with the Reynolds analogy and knowledge of the effect of turbulence on the velocity profile, it should be possible to predict the effect of turbulence intensity on heat-transfer rates.

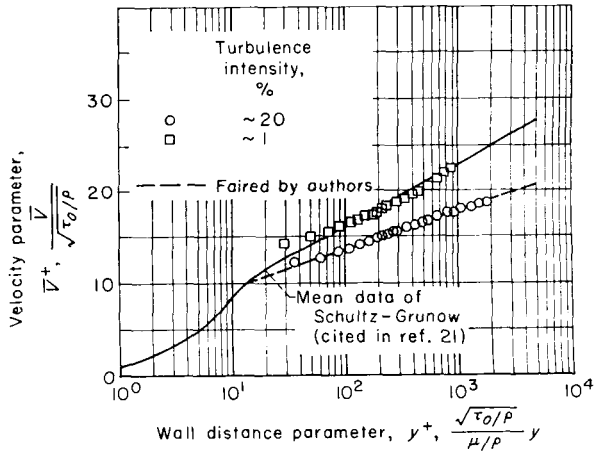

FIGURE 24.—Flat-plate velocity profiles (ref. 21).

A search of the literature revealed only one study on the effect of free-stream turbulence intensity on velocity profiles for a flat plate (ref. 21). These velocity profiles are shown in dimensionless form in figure 24 for free-stream turbulence intensities of about 1 and 20 percent and at a Reynolds number Re_x of 2×10^6. At the lower level of intensity, the data of reference 21 compared favorably with the "universal profile" obtained by Schultz-Grunow; however, at the higher level, a large deviation was observed, indicating that the profile was much flatter in the outer region of the boundary layer and, therefore, steeper at the wall.

These two profiles, faired as shown in figure 24, were used in the expression given by reference 19 to estimate the effect of turbulence intensity on heat-transfer rates. Although the profiles were obtained for a flat plate, it was assumed that the relative effect would be similar even though the expression was derived for pipe flow. The re-

sults so obtained indicated that the Nusselt number for a 20-percent turbulence intensity was about 60 percent larger than that for a 1-percent turbulence intensity. Thus, from analytical considerations and measured velocity profiles, it can be implied that heat-transfer rates increase with turbulence intensity in agreement with the observations of the present study. It has also been observed experimentally that the heat-transfer rates from a cylinder (e.g., refs. 22 and 23) and from a flat plate (ref. 24) increase with increasing free-stream turbulence intensity. In a more recent study of the flat plate, it was found that the heat-transfer rate increased with free-stream turbulence intensity only in the presence of a favorable pressure gradient (ref. 25). With a zero pressure gradient, no effect other than an earlier transition to turbulent flow was observed with increasing free-stream turbulence; however, the turbulence intensity was small, ranging from about 0.4 to 1.7 percent.

From the experimental relation given by equation (21) or (22), it is possible to generate curves of Nusselt number against Reynolds number at constant percentage ϵ. Typical curves are shown in figure 25 for station 2 at several values of ϵ. At the lower limit ($\epsilon=0$) the correlation gives the laminar-flow heat-transfer relation as shown. Experimental data were not obtained for values of ϵ less than 10 percent, and thus the curves for $0<\epsilon<10$ percent were obtained through extrapolation of the data to the laminar-flow case as discussed in the section entitled "Correlation of Data." The assumption made in the extrapolation was that the transition from laminar to turbulent flow was continuous and not characterized by a sudden change.

For comparison with the curves predicted by the correlation obtained in the present study, a curve, typical of the usual turbulent heat-transfer data found in the literature, is also shown in figure 25. The curve was computed for station 2 from an empirical equation for the flat plate with unheated starting length in turbulent flow (ref. 17).

Since the Reynolds number range covered in this study was relatively small, it is uncertain how far the predicted curves may be safely extrapolated. For this reason, no particular significance is attached to the indications of possible crossover points occurring at various Reynolds numbers and turbulence intensities.

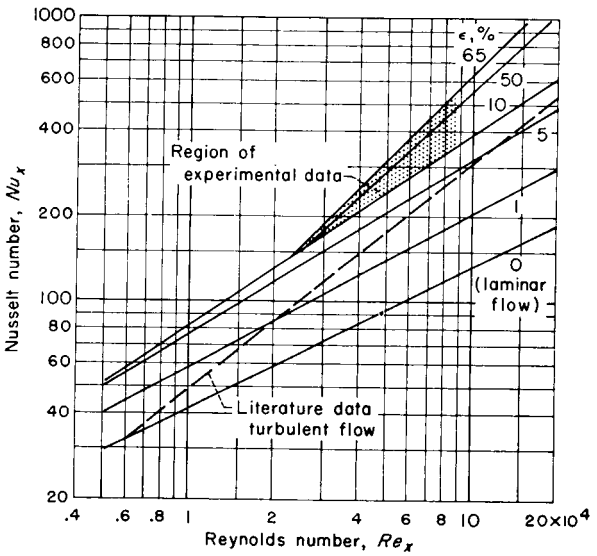

FIGURE 25.—Nusselt-Reynolds number relation from correlation expression. Station 2.

Provided that the turbulence intensity were known, the present correlation could predict the reference curve shown in figure 25. Unfortunately, this parameter has not generally been determined in heat-transfer studies. The trend shown in figure 25 for the reference curve compared with that predicted by this study requires that the turbulence intensity increase with Reynolds number or flow rate (i.e., the level of turbulence generated in wind-tunnel flow should increase with flow velocity). Such a trend is shown by the data of reference 26, where for extremely low intensities the turbulence intensity was observed to increase about twofold as the mean velocity was increased from 30 to 120 feet per second. Although the maximum increase in Nusselt number due to oscillations found in the present experiment was only about 65 percent, it should be noted again that the reference flow, on which this comparison is based, was highly turbulent; and because of this turbulence level the resulting heat-transfer rate is therefore believed to be larger than would ordinarily occur.

The trends predicted by the correlation of the data presented have indicated the importance of the level of turbulent energy or its equivalent, the root-mean-square flow amplitude, in determining heat-transfer rates. The more complicated second-order phenomena (refs. 1 and 2) that have been suggested in the past to explain the effects

of sound waves on heat-transfer rates appear to be unnecessary in the present work.

SUMMARY OF RESULTS

The following results were obtained from the experimental study of the heat transfer from a flat plate to an airstream having large-amplitude flow oscillations or a high degree of free-stream turbulence:

1. The heat-transfer coefficient was increased by as much as 65 percent with oscillations compared with the coefficient without oscillations. The reference flow on which this comparison is based was highly turbulent (10-percent turbulence intensity), and it is believed that for this reason the resulting heat-transfer coefficient is larger than that ordinarily obtained in turbulent flows.

2. An empirical correlation of the data was obtained for constant Prandtl number in the form $Nu_x = f_1(\epsilon) Re_x^{f_2'(\epsilon)}$ where $f_1(\epsilon)$ and $f_2'(\epsilon)$ are both functions of the ratio of the root-mean-square flow rate to the time-averaged flow rate, and Nu_x and Re_x are the Nusselt and Reynolds numbers, respectively. This expression correlated the data for turbulent flow as well as oscillating flow. At the lower limit, for no flow fluctuation, the expression reduces to that for laminar flow.

3. Over the frequency range (34 to 680 cps) studied, no effect of frequency was observed that could not be explained by consideration of other parameters.

4. Schlieren studies of the boundary layer revealed that flow reversal occurred near the wall at all frequencies during a part of the period of oscillation. Time-averaged schlieren measurements of the boundary-layer thickness showed that the thickness decreased in proportion to the increase in heat-transfer coefficient. From high-speed motion pictures of the boundary layer, obtained with a modified schlieren system, it was found that the gradient of the temperature or the temperature profile varied in a periodic manner.

5. The heat-transfer data obtained with flow oscillations appear to support a turbulence mechanism as the reason for the increased heat-transfer coefficient.

LEWIS RESEARCH CENTER
NATIONAL AERONAUTICS AND SPACE ADMINISTRATION
CLEVELAND, OHIO, *March 1, 1962*

REFERENCES

1. Westervelt, P. J.: Effect of Sound Waves in Heat Transfer. Jour. Acoustical Soc. Am., vol. 32, no. 3, Mar. 1960, pp. 337–338.
2. Fand, R. M., and Kaye, J.: The Effect of High Intensity Stationary and Progressive Sound Fields on Free Convection from a Horizontal Cylinder. TN 59–18, WADC, 1959.
3. Lemlich, R.: Vibration and Pulsation Boost Heat Transfer. Chem. Eng., vol. 68, no. 10, May 15, 1961, pp. 171–177.
4. Kestin, J., Maeder, P. F., and Wang, H. E.: On Boundary Layers Associated with Oscillating Streams. Brown Univ., Oct. 1959.
5. Illingworth, C. R.: The Effects of a Sound Wave on the Compressible Boundary Layer on a Flat Plate. Jour. Fluid Mech., vol. 3, pt. 5, Feb. 1958, pp. 471–493.
6. Lighthill, M. J.: The Response of Laminar Skin Friction and Heat Transfer to Fluctuations in the Stream Velocity. Proc. Roy. Soc. (London), ser. A, vol. 224, no. 1156, June 9, 1954, pp. 1–23.
7. Harrje, David T., and Croke, E. J.: Heat Transfer in Oscillating Flow. Rep. 483, Dept. Aero. Eng., Princeton Univ., Oct. 3, 1959.
8. Lemlich, Robert, and Hwu, Chung-Kong: The Effect of Acoustic Vibration on Forced Convective Heat Transfer. A.I.Ch.E. Jour., vol. 7, no. 1, Mar. 1961, pp. 102–106.
9. Romie, Fred E.: Heat Transfer to Fluids Flowing with Velocity Pulsations in a Pipe. Ph. D. Thesis, Univ. Calif., 1956.
10. Jackson, Thomas W., Purdy, Kenneth R., Oliver, Calvin C., and Johnson, H. L.: The Effects of Resonant Acoustic Vibrations on the Local and Overall Heat Transfer Coefficients for Air Flowing Through an Isothermal Horizontal Tube. TR 60–322, Aero. Res. Lab., Georgia Inst. Tech., Oct. 1960.
11. Raben, I.: The Use of Acoustic Vibrations to Improve Heat Transfer. Paper presented at Meeting of Heat Transfer and Fluid Mech. Inst., Univ. Southern Calif., June 1961.
12. Anantanarayanan, R., and Ramachandran, A.: Effect of Vibration on Heat Transfer from a Wire to Air in Parallel Flow. Trans. ASME, vol. 80, no. 7, Oct. 1958, pp. 1426–1432.
13. Kubanskii, P. N.: The Effect of Acoustic Streaming on Convective Heat Exchange. Soviet Phys. (Acoustics), vol. 5, 1959, pp. 49–55.
14. Laurence, James C., and Landes, L. Gene: Auxiliary Equipment and Techniques for Adapting the Constant-Temperature Hot-Wire Anemometer to Specific Problems in Air-Flow Measurements. NACA TN 2843, 1952.
15. Beams, J. W.: Physical Measurements in Gas Dynamics and Combustion. Vol. IX of High Speed Aerodynamics and Jet Propulsion, R. W. Ladenburg, ed., Princeton Univ. Press, 1954.

16. Sandborn, Virgil A., and Slogar, Raymond J.: Longitudinal Turbulent Spectrum Survey of Boundary Layers in Adverse Pressure Gradients. NACA TN 3453, 1955.

17. Hartnett, J. P., Eckert, E. R. G., Birkebak, Roland, and Sampson, R. L.: Simplified Procedures for the Calculation of Heat Transfer to Surfaces with Non-Uniform Temperatures. TR 56-373, WADC, Dec. 1956.

18. Bayley, F. J., Edwards, P. A., and Singh, P. D.: The Effect of Flow Pulsations on Heat Transfer by Forced Convection from a Flat Plate. Paper presented at Int. Heat Transfer Conf., Boulder (Colo.), Aug. 28–Sept. 1, 1961.

19. Deissler, Robert G.: Analytical Investigation of Turbulent Flow in Smooth Tubes with Heat Transfer with Variable Fluid Properties for Prandtl Number of 1. NACA TN 2242, 1950.

20. Deissler, Robert G.: Analytical and Experimental Investigation of Adiabatic Turbulent Flow in Smooth Tubes. NACA TN 2138, 1950.

21. Kline, S. J., Lisin, A. V., and Waitman, B. A.: Preliminary Experimental Investigation of Effect of Free-Stream Turbulence on Turbulent Boundary-Layer Growth. NASA TN D-368, 1960.

22. Kestin, J., and Maeder, P. F.: Influence of Turbulence on Transfer of Heat from Cylinders. NACA TN 4018, 1957.

23. Van Der Hegge Zijnen, B. G.: Heat Transfer from Horizontal Cylinders to a Turbulent Air Flow. Appl. Sci. Res., sec. A, vol. 7, nos. 2–3, 1958, pp. 205–223.

24. Sugawara, Sugao, Sato, Takashi, Komatsu, Hiroyasu, and Osaka, Hiroichi: The Effect of Free-Stream Turbulence on Heat Transfer from a Flat Plate. NACA TM 1441, 1958.

25. Kestin, J., Maeder, P. F., and Wang, H. E.: Influence of Turbulence on the Transfer of Heat from Plates with and without a Pressure Gradient. Paper presented at Int. Heat Transfer Conf., Boulder (Colo.), Aug. 28–Sept. 1, 1961.

26. Schubauer, G. B., and Skramstad, H. K.: Laminar-Boundary-Layer Oscillations and Transition on a Flat Plate. NACA Rep. 909, 1948.

TABLE I.—HEAT-TRANSFER—AMPLITUDE DATA

[Frequency, 46 cps.]

Rotor-stator spacing, in.	$\epsilon=\frac{(\rho V)_{rms}}{\rho V}$, percent	Station 2		Station 3	
		Nu_x	Re_x	Nu_x	Re_x
0.004	55.0	194	3.18×10^4	180	4.16×10^4
	62.1	298	4.45	288	5.82
	61.0	388	6.62	375	8.66
	63.0	392	6.23	376	8.15
	57.0	527	7.78	503	10.18
0.010	55.7	184	2.85×10^4	168	3.73×10^4
	56.6	279	4.80	266	6.28
	53.4	374	6.84	358	8.95
	57.4	453	7.39	443	9.68
	57.7	188	2.98	173	3.90
	57.9	282	4.58	274	6.00
	60.0	374	6.42	358	8.41
	56.9	475	7.45	473	9.75
	60.5	364	6.17	349	8.07
0.020	49.6	179	2.78×10^4	166	3.58×10^4
	49.2	267	4.61	257	6.03
	54.0	338	5.85	327	7.66
	53.8	445	7.32	433	9.58
	57.6	340	5.91	326	7.74
0.050	30.3	170	2.56×10^4	159	3.35×10^4
	37.1	268	4.90	257	6.41
	41.1	327	6.34	315	8.30
	39.7	389	7.21	375	9.44
	40.3	316	6.44	306	8.42

TABLE II.—HEAT-TRANSFER—FREQUENCY DATA

[Rotor-stator spacing, 0.004 in.]

Frequency, cps	$\epsilon=\frac{(\rho V)rms}{\overline{\rho V}}$, percent	Station 2		Station 3	
		Nu_x	Re_x	Nu_x	Re_x
34	53. 5	200	3.24×10^4	187	4.24×10^4
46	59. 9	218	3. 54	202	4. 63
98	43. 6	173	3. 14	157	4. 11
148	47. 8	188	3. 32	168	4. 35
210	30. 8	175	3. 03	164	3. 97
270	45. 6	170	3. 03	160	3. 97
427	35. 6	174	2. 79	166	3. 65
472	42. 7	185	3. 15	175	4. 12
540	28. 4	179	3. 16	169	4. 14
580	34. 8	178	3. 00	167	3. 92
680	40. 0	179	2. 85	167	3. 73
34	57. 5	276	4. 81	260	6. 30
46	60. 0	308	4. 75	293	6. 22
98	46. 0	262	4. 49	240	5. 87
148	55. 1	283	5. 26	273	6. 88
210	34. 0	256	4. 49	241	5. 87
270	59. 8	240	4. 07	225	5. 33
427	41. 1	238	4. 35	228	5. 69
472	51. 9	254	4. 59	247	6. 00
540	34. 0	230	4. 65	218	6. 07
580	45. 7	223	4. 67	218	6. 11
680	44. 4	231	4. 61	223	6. 04
34	59. 0	366	6. 45	348	8. 45
46	61. 3	411	6. 34	394	8. 28
98	48. 7	334	5. 48	313	7. 17
148	58. 2	401	6. 62	390	8. 66
210	35. 9	366	5. 45	361	7. 12
270	53. 9	332	5. 39	325	7. 04
427	42. 4	314	5. 51	319	7. 22
472	56. 6	325	5. 08	333	6. 65
580	51. 0	290	5. 47	304	7. 15
680	50. 5	294	5. 29	311	6. 92
34	60. 6	437	7. 54	405	9. 83
46	61. 6	505	7. 28	478	9. 52
98	47. 6	378	7. 28	358	9. 52
148	60. 4	524	8. 28	512	10. 83
210	35. 3	481	7. 02	443	9. 18
270	55. 5	411	7. 44	409	9. 72
472	56. 1	374	7. 50	393	9. 82
580	54. 4	328	7. 00	352	9. 15
680	49. 9	342	6. 85	382	8. 96

U.S. GOVERNMENT PRINTING OFFICE: 1963